Compact HTS Motor Designs Especially Useful to be Cooled by Liquid Hydrogen

Roberto A. H. de Oliveira, Othman Taalibi, Tabea Arndt

***Abstract*—HTS paved the way to power devices operated at elevated temperatures (e.g., LN_2). This reduced the required cooling efforts such that electric motors became an option for a number of applications. Nowadays, the consideration of LH_2 as a fuel in fuel-cell electric drivetrains is offering a temperature level of from $20\,K$ to $30\,K$ without additional cooling efforts. In these vehicle applications, the "for-free" cooling enables new concepts in electric machines. The Disk-Up-Down Assembling (DUDA) coil topology is introduced in this work for application in both fully and partially superconducting motors. With significant electromagnetic characteristics tailored for HTS motor design, this novel topology facilitates exploration of winding configurations in HTS motors. Preliminary results from our investigations are presented herein.**

***Index Terms*—superconductivity, hydrogen, HTS motors, DUDA coils.**

I. Introduction

SUPERCONDUCTING motors are extremely important in the electrification process of traction systems. Optimized superconducting electrical machines are useful to use of these ones in aircraft, ships, trucks, wind generators and others devices. The increase in power density is a desirable feature and the definitive solution for electric traction in the aviation sector. Hydrogen system allow an efficiency cooling and energy generation and based on these premises, this work presents simulation results for partially and fully superconducting motors with the innovative Disk-Up-Down Assembling (DUDA) coils [1]. The cooling system, the description of the topology of this newer coil topology, and the preliminary results of the HTS motors are presented. The machines have excellent torque range and AC losses were reduced through simple approaches presented in this work.

II. Hydrogen Cooling System

Hydrogen systems offer a temperature range between 15 and $40\,K$ serving a wide range of applications with superconductors. Liquid hydrogen (LH_2) has a boiling point slightly above $20\,K$, according to data in Table I [2]–[4], being very useful characteristic for cooling large-scale coils and windings due to its low viscosity and high latent heat ($443\,kJ\,kg^{-1}$). Refrigeration with gaseous hydrogen (GH_2) avoids problems related to volume expansion, due to the phase transition of hydrogen (liquid-gas), during an eventual quenching. Based on these considerations, two possible approaches to cool the proposed motor follow [5]–[7].

Figure 1 shows a cooling system with LH_2 and a fuel cell power generation. At this temperature level the superconductor presents higher critical currents, as well known. For a motor with $\eta = 0.95$ and shaft power of $1000\,kW$, considering the cold energy (LH_2-GH_2) of $1.24\,kW\,h\,kg^{-1}$ and the energy density of $33.3\,kW\,h\,kg^{-1}$, the input power to the fuel cell can be $1754.39\,kW$ with an efficiency of 60%. The fuel cell should provide an output power of $1052.63\,kW$. Figure 2 shows the system for cooling a HTS motor by GH_2. A motor developing output power of $600\,kW$ with an efficiency of 95%, the electrical input power to the drive will be $631.58\,kW$. This power will be supplied by the fuel cell (60% efficient), which would require an input power of $\approx 1050\,kW$.

TABLE I: Physical parameters of Hydrogen.

Parameter	LH_2	GH_2
Boiling Point	$20.3\,K$	-
Density	$70.8\,kg\,m^{-3}$	$1.338\,kg\,m^{-3}$
Specific Heat	$9.66\,kJ\,kg^{-1}\,K^{-1}$	$12.15\,kJ\,kg^{-1}\,K^{-1}$
Latent Heat	$443\,kJ\,kg^{-1}$	-
Viscosity	$132\,\mu Poise$	$11.28\,\mu Poise$
Critical Temp.	$32.97\,K$	-

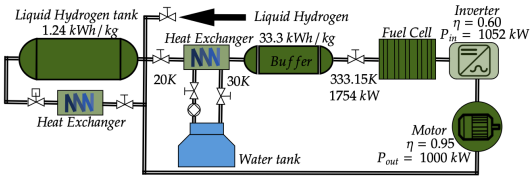

Fig. 1: LH_2 cooling system.

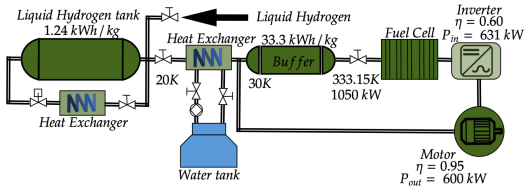

Fig. 2: Cooled motor by GH_2 system.

III. DUDA HTS Coil

The superconductor winding presented in this work has a configuration called DUDA in rectangular topology. This formation is given by connecting layers of HTS tapes oriented around the y axis, orthogonal to the xz plane, and connected to each other. This connection is made by a transversal cut in each strand that allows the connection of ends with the predecessor and the successor strand, as shown in Figure 3. Experimental tests with a rectangular DUDA coil were carried out and are presented in [1].

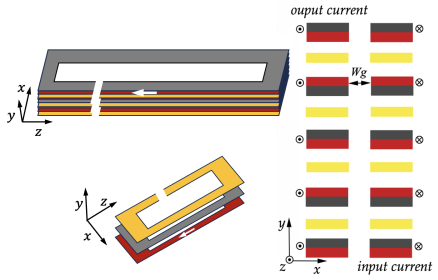

Fig. 3: DUDA rectangular coil. HTS Layers (red), Substrate (grey), Kapton (yellow) - *not scaled*.

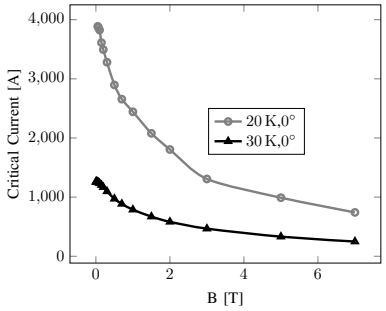

Fig. 4: Critical current versus magnetic flux density on 2G HTS tape in 20 K (Shanghai Creative Superconductor Technologies) and 30 K from Theva Pro-Line 2G HTS. The critical current curves were adjusted since they are affected by laser cutting and result in a reduction.

Specific advantages of the DUDA coil:

- Lower shear force for stacks with high numbers of turns and consequent reduction in winding delamination.
- The distribution of heat and therefore the cooling of the coils is facilitated in coils with a large number of turns, due to the bore between the coil legs and its topology.
- In windings applied to motors, we have an additional advantage, which is the elimination of coil heads. Despite the dimensions of coil heads in concentric or single-layer windings having reduced dimensions, the absence of this element inherent to motors reduces their dimensions and improves the thermal flow of the machine.

To mitigate AC losses on the coils, among other actions, one must promote the decoupling of magnetic flux density (B) in the bore, since it affects the tapes perpendicularly, maintaining the amplitudes of B suitable for each design. Furthermore, decreasing the current amplitude will reduce AC losses [8], [9]. Following this approach, the electromagnetic behavior and AC losses in two different topologies were evaluated and derived through numerical simulations. To this, DUDA coils was preformed with 2G tapes, supposing the realistic characterization according to Figure 4. Table II presents the main parameters of the coils. Magnetic field density in the coil with 1 branch per leg and 2 mm bore, fed by 90 A at 400 Hz is 4.8 times greater than the coil with 3 branches per leg under the same load conditions (Figure 5).

Motor design with DUDA winding must account for losses resulting from contact resistances. Experimental tests revealed the lowest measured contact resistance to be 12 nΩ. The total resistance of the 4-tape stack was determined to be 68 nΩ, equating to an average contact resistance of approximately 23 nΩ [10].

TABLE II: Data of DUDA rectangular coil

Parameter	Value	Parameter	Value
Width each leg	5 mm	Current	10 to 90 A
Width bore	2 to 10 mm	Frequency	50 to 400 Hz
Length of coil	1000 mm	N. of tape	50

The total loss of superconducting material can be calculated using (1) and the loss per cycle for periodic excitations of current by (2) [11], where $\mathbf{J}$ is the current density [Am^{-2}], $\mathbf{E}$ the electric field [Vm^{-1}], v the volume of the sample and $\mathbf{r}$ [m] the radial coordinate.

$$P = \int_v d^3\mathbf{r}\mathbf{J}\cdot\mathbf{E} \quad (1)$$

$$Q = \oint dt \int_v d^3\mathbf{r}\mathbf{J}\cdot\mathbf{E} \quad (2)$$

The **TA**-formulation referred to is commonly used to address and resolve issues related to superconductivity [12], [13]. This analysis approximates the HTS material's geometry to 1D, although the system being analyzed is built in 2D. Equation (3) governs the **T**-formulation, which describes the current inside the superconducting material through manipulating Faraday's law (4) and the definition of current density (5).

$$\nabla\times\rho\nabla\times\mathbf{T} = -\frac{\partial\mathbf{B}}{\partial t} \quad (3)$$

$$\mathbf{J} = \nabla\times\mathbf{T} \quad (4)$$

$$\nabla\times\rho\mathbf{J} = -\frac{\partial\mathbf{B}}{\partial t} \quad (5)$$

In the region surrounding the HTS material under analysis, the field behaviour can be expressed by (6) that is the **A**-formulation. The equation originates from (7) and (8), Ampere's Law and the magnetic vector potential definition. **TA**-formulation combines these two calculation approaches and guarantees an accurate solution. **T** and **A** are fully coupled because are solved at the same time, once time eddy current is present in motors. The interface boundary should be considered carefully.

$$\nabla\times\frac{\nabla}{\mu_0}\times\mathbf{A} = \mathbf{J} \quad (6)$$

$$\nabla\times\mathbf{B} = \mu_0\mathbf{J} \quad (7)$$

$$\mathbf{B} = \nabla\times\mathbf{A} \quad (8)$$

Figure 6 shows the AC losses results in DUDA coils and dependence on temperature [14]. Operation at 20 K is more suitable than at 30 K due reduced losses, although just slightly lower. A coil with 3 branches in parallel at T=30 K has 79.16 % lower losses than coil with 1 branch, 50 W and 240 W, respectively. The influence of the magnetic field

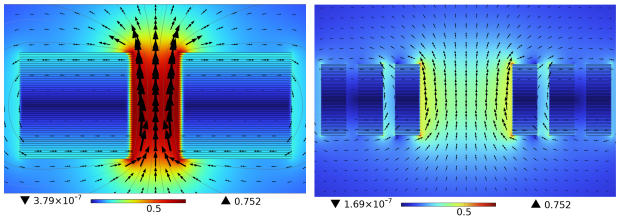

Fig. 5: Magnetic flux density on DUDA coil 50 tapes and current applied of 90 A at 400 Hz. Left figure presents width bore 2 mm and right figure has , width bore 10 mm and distance between branches is 0.75 mm.

decoupling on the AC losses can be seen from Figure 6, where the simulation was carried out on the coil with 1 branch per leg and a bore width of 2 mm and 10 mm, fed by 90 A at 400 Hz.

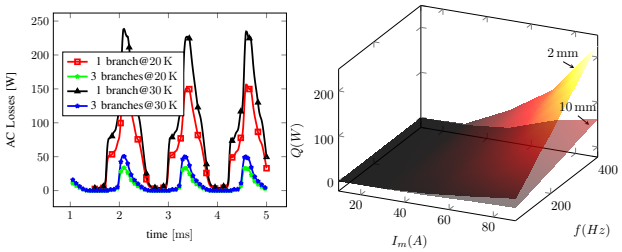

Fig. 6: AC losses on coils fed by 90 A at 400 Hz, 20 K and 30 K in the coils described on Table II (left side). AC losses on a DUDA rectangular coil with a bore width of 2 mm and 10 mm (right side).

IV. HTS Motors

This section presents superconducting motors designed for liquid and gaseous hydrogen-cooled systems. The classical electric machine design approach was used in both motors, however fully superconducting motor require adaptations in the design stages. Armature winding design considered the AC losses approach performed in the section III [11].

A. Partial HTS Motor

A partially superconducting motor was designed using a classical approach to determine the main dimensions, taking into account desired magnetic field density values in the air gap. The linear current density in the motor stator is defined by (9) and the tangential stress (σ_{Ftan}) that produces the torque of the machine when acting upon the rotor surface, shown in (10) [15]–[17].

$$A = \frac{I_1 z_Q}{\tau_1}[\mathrm{kAm^{-1}}], \qquad \tau_1 = \frac{\pi D}{Q_1}[\mathrm{m}] \tag{9}$$

$$\sigma_{Ftan} = \frac{\hat{A}\hat{B}_g \cos(\varphi)}{2} = \frac{A\hat{B}_g \cos(\varphi)}{\sqrt{2}}[\mathrm{Nm^{-2}}] \tag{10}$$

where I_1 is the RMS stator current, z_Q the number of conductors in the slot with all turns in series, τ_1 the stator slot pitch, D the diameter around the middle of the airgap (can be used inner diameter of the stator or the outer diameter of the rotor), Q_1 the number of slots in the stator, A the linear current density, $\hat{A}$ is the sinusoidal linear current density peak, $\hat{B}_g$ the sinusoidal airgap flux density peak, φ is the lagging between $\hat{A}$ and $\hat{B}$ in synchronous machines is 0 and A the RMS value of $\hat{A}$.

Table III shows the main data of the motor. The dimensions of the tooth and slot of the motor are shown in Figure 7. The magnetic package is formed by sheets of laminated ferromagnetic material, distributed stranded winding in a single layer and the current density J=4.2 A mm^{-2}.

TABLE III: Data of Partial HTS Motor

Parameter	Value	Parameter	Value
Phase current rms	420 A	Outer diam.	250 mm
Phase voltage	350 V	Inner diam.	150 mm
Output power	0.6 MW	Length	500 mm
Torque	6 kN m	Airgap	5 mm
Speed	1000 rpm	N. of poles	16

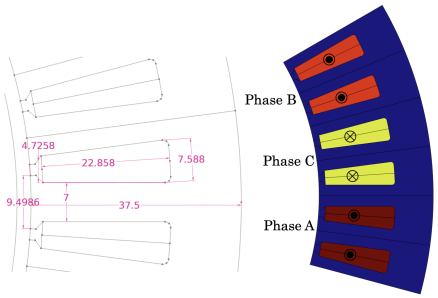

Fig. 7: Slot and tooth dimension of the stator on partial HTS motor.

The rotor used rectangular DUDA coils in Halbach formation. The coils have a different number of turns with 65 turns in the ends and center packages (composed of tapes that are 10 mm wide and have a 2 mm central bore) but 48 turns in the other two coils group of the formation (4 mm wide and 0.6 mm central bore), and fed by 200 A. The presented results are based on the operation at 20 K. Figure 8 shows the formation of the poles and the current density normalized.

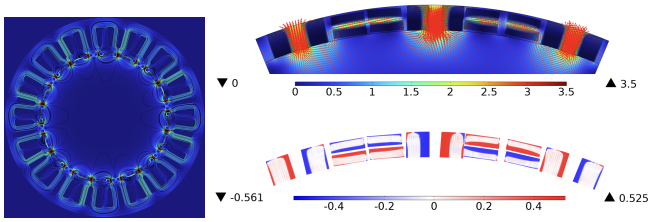

Fig. 8: Motor and DUDA coil Halbach. Magnetic flux density [T] (right top) and $Jz/J_c(B)$ (right bottom).

Figure 9 shows the torque curve as a function of the initial electrical angle of the motor. The maximum torque is 10 kN m at an angle of 74° and the nominal torque is 6 kN m for operation at unity power factor (Figure 9).

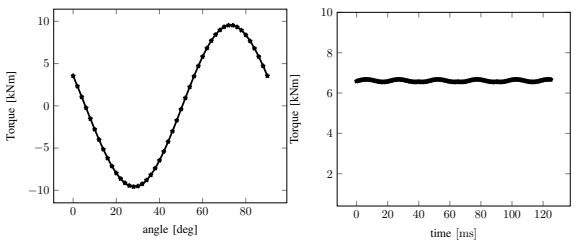

Fig. 9: Torque versus angle (left) and nominal torque (right) on the partial HTS motor.

B. Fully HTS Motor

A fully superconducting three-phase motor for operation with GH_2 or LH_2 was designed and its main dimensions are shown in Table IV. This motor has a primary (stator) and secondary (rotor) winding made with 2G HTS tapes, the characterization of which is given in Figure 4. The stator has 3 branches in parallel with the aim of reducing AC losses. In addition, teeth were added to the stator although with the yoke, their are additional sources of losses, negligible compared to the winding. The teeth reduce reluctance and the incidence of the magnetic field on the tapes, thus reducing AC losses. The topology of the winding and teeth was optimized in order to reduce AC loss. The winding with flat and curved configurations are illustrated in Figure 10, where a plane coil is showed ($0°$), inclined coil $20°$ and declined coil ($-20°$). The curved coil reduces the losses by reducing the angle of incidence of the magnetic field, which presents maximum loss when the incidence is $90°$. The multi-objective function was established by considering variables such as coil curvature and the tooth geometry, which refers to the volume and shape of the tooth. The optimization process relied on deterministic algorithms using a simple approach, involving both maximization and minimization to identify the optimal points. The radius adopted for each stack of tapes was $25\,\mathrm{mm}$. The winding teeth are designed to best accommodate the winding in each case.

TABLE IV: Data of Fully HTS Motor

Parameter	Value	Parameter	Value
Turns stator	181 per coil	Outer diam.	497 mm
Turns rotor	81 per coil	Inner diam.	406 mm
Output power	≈1 MW	Length	800 mm
Torque	≈10 kN m	Airgap	1 mm
Speed	1000 rpm	N. of poles	32

Figure 11 presents the simulation results for a quarter of the superconducting motor geometry. Magnetic flux density in teeth with a plane coil (see Figure 10) is slightly saturated and the magnetic flux in the air gap is quite high. This characteristic promotes high torque, as shown in Figure 12. AC losses with a inclined coil are 27% lower than with a plane coil. Losses can be reduced by 46% at the temperature of 30 K if the plane coil is replaced by declined coil. Refrigeration with LH_2 and declined winding guarantees acceptable losses levels for a refrigeration system.

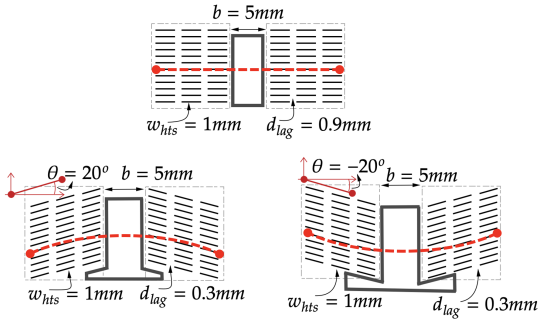

Fig. 10: Tooth shapes of the stator on fully HTS motor. Plane winding ($0°$) on top, inclined winding ($20°$) on left, and declined winding ($-20°$) on right.

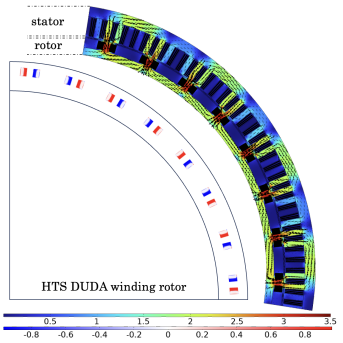

Fig. 11: Fully HTS motor. Magnetic flux density and normalized density current.

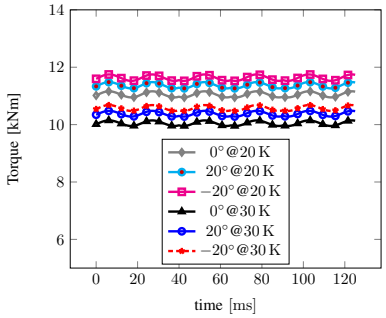

Fig. 12: Nominal torque on the partial HTS motor.

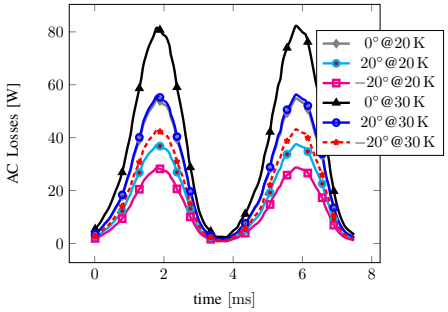

Fig. 13: AC Losses @20 K and 30 K.

V. Conclusions

This preliminary study indicates the possibility of operating superconducting motors (partial and fully) in LH_2 and GH_2

cooling using DUDA coils. GH_2 is simpler than LH_2 due to issues related to the hydrogen phase transition. However, the reduction of AC losses can be slightly improved with LH_2. The insertion of iron teeth into the stator may seems a priore unnecessary, as it is a source of additional losses, but it might reduce AC losses due to the reduction of field c urrent and magnetic flux i ncident o n t he a rmature winding.

REFERENCES

[1] T. Arndt, B. Holzapfel, M. Noe, R. Nast, F. Hornung, M. Kläser, and A. Kudymow, "New coil configurations with 2G-HTS and benefits for applications," *Superconductor Science and Technology*, vol. 34, no. 9, p. 095006, Sep. 2021. [Online]. Available: https://iopscience.iop.org/article/10.1088/1361-6668/ac19f4

[2] M. Conte, A. Iacobazzi, M. Ronchetti, and R. Vellone, "Hydrogen economy for a sustainable development: state-of-the-art and technological perspectives," *Journal of Power Sources*, vol. 100, no. 1-2, pp. 171–187, Nov. 2001. [Online]. Available: https://linkinghub.elsevier.com/retrieve/pii/S037877530100893X

[3] M.-C. Bellissent-Funel and J. C. Dore, Eds., *Hydrogen Bond Networks*. Dordrecht: Springer Netherlands, 1994. [Online]. Available: http://link.springer.com/10.1007/978-94-015-8332-9

[4] "Hydrogen fuel cell engines and related technologies: Rev 0, december 2001," https://www1.eere.energy.gov/hydrogenandfuelcells/tech_validation/pdfs/fcm01r0.pdf, accessed: 2023-09-20.

[5] S. Hara, Y. Iwami, R. Kawasaki, T. Matsumoto, Y. Shirai, M. Shiotsu, H. Kobayashi, Y. Naruo, S. Nonaka, Y. Inatani, M. Ishii, S. Yoshinaga, and T. Tanaka, "Development of Liquid Hydrogen Cooling System for a Rotor of Superconducting Generator," *IEEE Trans. Appl. Supercond.*, vol. 31, no. 5, pp. 1–5, Aug. 2021. [Online]. Available: https://ieeexplore.ieee.org/document/9376909/

[6] M. Mojarrad, S. Farhoudian, and P. Mikheenko, "Superconductivity and Hydrogen Economy: A Roadmap to Synergy," *Energies*, vol. 15, no. 17, p. 6138, Aug. 2022. [Online]. Available: https://www.mdpi.com/1996-1073/15/17/6138

[7] M. Sander, R. Gehring, and H. Neumann, "LIQHYSMES—A 48 GJ Toroidal MgB2-SMES for Buffering Minute and Second Fluctuations," *IEEE Trans. Appl. Supercond.*, vol. 23, no. 3, pp. 5 700 505–5 700 505, Jun. 2013. [Online]. Available: http://ieeexplore.ieee.org/document/6384697/

[8] A. Godfrin, *AC Losses in High-Temperature Superconductor Tapes and Cables for Power Applications*. KIT Scientific Publishing, 2022. [Online]. Available: https://publikationen.bibliothek.kit.edu/1000131627

[9] E. Pardo, F. Grilli, Y. Liu, S. Wolftadler, and T. Reis, "AC Loss Modeling in Superconducting Coils and Motors With Parallel Tapes as Conductor," *IEEE Trans. Appl. Supercond.*, vol. 29, no. 5, pp. 1–5, Aug. 2019. [Online]. Available: https://ieeexplore.ieee.org/document/8641334/

[10] A. Huber, "Studie zum Einsatz von durchgehend kontaktierten Hochtemperatursupraleiter-Bandstapeln in kompakten Magneten," Ph.D. dissertation, Karlsruher Institut für Technologie, Nov. 2023.

[11] B. Dutoit, F. Grilli, and F. Sirois, "Numerical Modeling of Superconducting Applications: Simulation of Electromagnetics, Thermal Stability, Thermo-Hydraulics and Mechanical Effects in Large-Scale Superconducting Devices," Singapore: World Scientific, Mar. 2023. [Online]. Available: https://www.worldscientific.com/worldscibooks/10.1142/13282

[12] H. Zhang, M. Zhang, and W. Yuan, "An efficient 3D finite element method model based on the *T–A* formulation for superconducting coated conductors," *Supercond. Sci. Technol.*, vol. 30, no. 2, p. 024005, Feb. 2017. [Online]. Available: https://iopscience.iop.org/article/10.1088/1361-6668/30/2/024005

[13] E. Berrospe-Juarez, F. Trillaud, V. M. R. Zermeno, and F. Grilli, "Electromagnetic modeling of large-scale high-temperature superconductor systems," *arXiv*, 2020. [Online]. Available: https://arxiv.org/abs/2006.02033

[14] J. Kováč, Kopera, E. Pardo, T. Melišek, R. Ries, E. Berberich, S. Wolfstädler, and T. Reis, "Measurement of AC loss down to 25 K in a REBCO racetrack coil for electrical aircraft motor," *Sci Rep*, vol. 12, no. 1, p. 16454, Sep. 2022. [Online]. Available: https://www.nature.com/articles/s41598-022-20625-6

[15] J. Gieras, *Advancements in Electric Machines*, ser. Power Systems. Springer Netherlands, 2008. [Online]. Available: https://books.google.de/books?id=FzHgWqRZ_moC

[16] E. Arnold, J. L. La Cour, and A. Fraenckel, *Die wechselstromtechnik*. Springer, 1904, vol. 1.

[17] J. Pyrhonen, T. Jokinen, and V. Hrabovcová, *Design of Rotating Electrical Machines*, 2nd ed. Chichester, West Sussex, United Kingdom: Wiley, 2014.